Microstructure and Weibull distribution of rupture strength of clay-talc ceramics

(Microestrutura e distribuição de Weibull da resistência à ruptura de cerâmicas de argila-talco)

L. Zerbo[1]*, M. Seynou[1], B. Sorgho[1], G. Lecomte-Nana[2], M. Gomina[3], P. Blanchart[2]

[1]*Université Ouaga I Professeur Joseph Ki-Zerbo, U.F.R-S.E.A, Laboratoire de Chimie Moléculaire et des Matériaux, 03 BP 7021 Ouagadougou 03, Burkina Faso*

[2]*Institute of Research for Ceramics (IRCER), UMR-CNRS 7315, Limoges, Cedex, France*

[3]*CRISMAT, UMR 6508, Ensicaen, Equipe Structure et Comportement Thermomécanique des Matériaux, Caen Cedex, France*

Abstract

The mechanical properties of clay-talc ceramics containing 0 to 10 wt% of talc fired at 1100 °C were obtained by flexural measurements. With the average value of flexural strength of 23.1 MPa, the sample with 5 wt% of talc (G5) was the strongest and it had the lowest value of interconnected pore (64%). The scattering of strength values was described with the Weibull distribution model. For all samples, Weibull plots showed either a typical linear behavior or a multi-stage response and the Weibull modulus varied in a large range of 3 to 14, depending on the ceramic type and on the applied load. Interconnections between pores formed a network of possible failures under the stress field, resulting in a change of Weibull plots. Reducing the grain size range and the pore interconnectivity led to a reduced strength distribution. The flaw size range had a unimodal distribution for sample G5 with homogeneous microstructure and correspondingly a Weibull modulus m=9.79.

Keywords: ceramic matrix, microstructural characteristics, Weibull statistic, mechanical properties.

Resumo

As propriedades mecânicas das cerâmicas de argila-talco contendo 0 a 10% em massa de talco sinterizadas a 1100 °C foram obtidas por medidas de flexão. Com o valor médio de resistência à flexão de 23,1 MPa, a amostra com 5% de talco (G5) foi a mais forte e apresentou o menor valor de poro interconectado (64%). A dispersão dos valores de resistência foi descrita com o modelo de distribuição de Weibull. Para todas as amostras, os gráficos de Weibull mostraram um comportamento típico linear ou uma resposta de múltiplos estágios e o módulo de Weibull variou em uma ampla faixa de 3 a 14, dependendo do tipo de cerâmica e da carga aplicada. Interconexões entre poros formaram uma rede de possíveis falhas sob o campo de tensão, resultando em uma mudança nos gráficos de Weibull. Reduções da faixa de tamanho dos grãos e da interconectividade dos poros levaram a uma redução na distribuição da resistência. A faixa de tamanho de defeito apresentou uma distribuição unimodal para a amostra G5 com microestrutura homogênea e correspondentemente um módulo de Weibull m=9,79.

***Palavras-chave**: matriz cerâmica, características microestruturais, estatística de Weibull, propriedades mecânicas.*

INTRODUCTION

Ceramics for the building are heterogeneous and porous materials often composed of clay sand mixtures that are consolidated by firing at 1000-1200 °C [1]. For a given composition, the mechanical properties are controlled by the microstructural characteristics, i.e. phase distribution, size of sand grains and pore size distribution [2]. Fracture of brittle materials, like ceramics, usually initiates from flaws. Brittle fracture is controlled by microscopic inclusions, surface and interior flaws and defects, as well as pores of different sizes and shapes, present in the sintered material arising from the manufacturing process [3, 4]. When fabricating clay products (e.g. bricks, roof tiles, floor tiles), the starting particle size distribution and the particle arrangement during the shape forming and firing process changes the particle size and porosity distribution in the fired microstructure. In microstructures, rigid assemblies of sand grains with fired clay can be disaggregated under stress into small clusters. Multiple fracture processes at a small scale in the fired clay between large grains occurs, and the breakage of internal bonds leads to macroscopic rupture mechanisms [5]. It extensively changes the mechanical properties under constant pressure due to construction.

In general, a statistical approach to mechanical properties

is used due to the random nature of rupture mechanisms in ceramics. They arise from the local defect at small scale inducing the breakage of larger particle linkages. Weibull statistics has been widely used to describe the statistical behavior of mechanical properties of many materials, such as advanced ceramics, glass, metallic matrix composites, ceramic matrix composite and polymeric matrix composites [1, 5, 6]. In this study, we studied the behavior of common silicate ceramics composed of clay-talc mixtures, in relation to microstructural characteristics. Strength variations under different stresses were determined with the Weibull statistical approach. Since these very simple materials are extensively used around the world, their mechanical properties must be improved to open new perspectives in building methods and in the durability of construction. This work aims at contributing in this direction.

MATERIALS AND METHODS

The two mineral materials used were clay and talc mined in Burkina Faso. They were from quarries that operate for a long time by local users. The SIT (Sitiéna) clay is mined near Banfora city and the Gar talc is mined near Garango city. Chemical compositions and properties of both mineral materials were already reported [7, 8]. Mineralogical compositions were obtained by X-ray diffraction using a Bruker D5000 diffractometer operating at 40 kV-40 mA and using the monochromatic CuKα radiation. The analysis of X-ray diffraction pattern according to ASTM (American Standards for Testing Materials) with open database resulted in the phase identification. Using both chemical and mineralogical analysis, we were able to semi-quantify the identified minerals, the results of which are recorded in the Table I. Powders of minerals were obtained by dry grinding and sieving at 100 μm. Grain size distributions were determined with a Malvern 2000 laser particle size analyzer by the wet method, and main data are reported in Table I. It is seen that talc granulometry was much larger than that of clay minerals. Besides, it is supposed that quartz in clay and dolomite in talc are granular phases with the largest grain sizes.

Three different clay-talc mixtures were obtained by soft ball milling with a Fritsch planetary mixer, to limit the grain size reduction, but attaining a high homogeneity at the grain scale. Mixture compositions are reported in Table II. Mineral material mixtures were shaped by die pressing (25 MPa) of dry granulated powders to form flat tiles (50x50x6 mm). After drying at 100 °C, tiles were fired at 1100 °C during 0.5 h (electric kiln, air atmosphere) with heating and cooling rates of 3 °C.min^{-1}.

Table II - Compositions of clay-talc ceramics.
[Tabela II - Composições das cerâmicas de argila-talco.]

Mixture	Clay (wt%)	Talc (wt%)
G0	100	0
G5	95	5
G10	90	10

Weibull statistics is a specific approach within the large thematic dedicated to rupture strength. It relates the behavior of fragile materials to their microstructural characteristics [9]. In the Weibull approach, the statistical treatment is based on the hypothesis of the existence of weakest links within assemblies of connected links in the material. Macroscopic fracture occurs with the rupture of the weakest link [10]. In the volume V made of n elements within a volume V_o, and under a stress σ_r, the probability of failure is:

$$P(V_o) = 1 - \exp\left[-\left(\frac{\sigma_r - \sigma_u}{\sigma_0}\right)^m\right] \qquad (A)$$

where σ_0 is the characteristic strength, σ_u is the stress below which the probability of failure tends to zero and m is the modulus of Weibull that is a measure of the variability of the strength of the material. In brittle materials, $\sigma_u=0$ is assumed because fracture can occur even at very low-stress level. It is an arbitrary assumption which is simply adopted because it is a conservative assumption. It allows easier parameter estimation in Eq. A. In the literature, it was proposed numerous approaches for obtaining Weibull parameters, and the most often used are [11-14]: moment generating function; maximum-likelihood estimation; and linear regression function. The last one is the simplest but sufficiently significant method, providing that a large number of samples are tested. Eq. A can be rearranged in the form:

$$\ln[-\ln(1-P_r)] = m\ln\sigma_r - m\ln\sigma_0 \qquad (B)$$

Eq. A relates the probability of rupture and the maximum stress which can be applied to a sample. It is in the form of a linear relation having a slope m and a Y-intercept of $-m\ln\sigma_0$. P_r is the unknown parameter related to experimental data. It is given using a statistical estimator, which can be defined under different forms. The most relevant form is the following, whereas it requires a large number of samples [4]:

$$P_{r,i} = \frac{i}{n+1} \qquad (C)$$

Table I - Mineralogical compositions (wt%) of the clay and talc.
[Tabela I - Composições mineralógicas (% em massa) da argila e do talco.]

	Kaolinite	Illite	Montmorillonite	Albite	Orthoclase	Talc	Chlorite	Dolomite	Quartz	Granulometry d$_{90}$
Clay	19%	11%	26%	16%	7%	-	-	-	13%	25 μm
Talc	-	-	-	-	-	77%	14%	8%	-	136 μm

for the sample i in the whole set of n samples. In general, at least 50 samples are required to reduce the estimated error down to 10%. Different estimators were also proposed, which are still valid with only 20 samples, but the general assessment indicates a number of 30 samples. For a set of n samples, values of peak constrain (σ_r) are arranged increasingly. The experimental plot of $\ln[-\ln(1-P_r)]$ against $\ln\sigma_r$ can be approximated by linear regression, giving the Weibull parameter m. The most important difficulty is the experimental needing of a large set of samples to be tested, to ensure the statistical significance of m.

Flexural mechanical properties are obtained by three-point flexure test where a specimen with a round, rectangular or flat cross-section is placed on two parallel supporting pins. A loading force is applied in the middle by means of a loading pin. The supporting and loading pins are mounted in the way to allow their free rotation about the axis parallel to the pin axis. This configuration provides uniform loading of the specimen and prevents friction between the specimen and the supporting pins. The fracture strength was obtained with samples having a width of B=8 mm and a thickness of W=6 mm. We used a 3-point bending fixture with a support span of L=40 mm. The testing apparatus was an Instron type equipped with a load cell of 10 kN and was piloted with Bluehill 2 software. The cross-head speed was 3 mm/min. Maximum load at failure (F_r) were converted to rupture strength (σ_r) from the usual relation valid for rectangular samples:

$$\sigma_r = \frac{3}{2}\frac{LF_r}{BW^2} \qquad\qquad (D)$$

Toughness values where obtained from flexural strength considering that for brittle ceramics large pores are initiating cracks and have a leading role in material applications [15]. The linear elastic fracture provides a relation between the length of the crack a and the rupture stress (σ_r) [16]:

$$K_{Ic} = Y\sigma_r\sqrt{a} \qquad\qquad (E)$$

where K_{Ic} is the fracture toughness at the local scale and Y a shape factor depending on the shape of cracks. For a common crack plane, Y is close to unity and a similar value is assumed for the internal surface of elongated pores [15].

For microstructural analysis, the fractured surfaces of the specimens after three-point bending tests were polished and examined by scanning electron microscopy (SEM). Carbon was vaporized under vacuum on material surfaces before recording SEM images. Microstructure observations of the specimen were carried out using a Jeol Hitachi SC 2500 scanning electron microscope. For observations and measurements, we acquired 10 images from 3 samples of each ceramic type to ensure that the deviation of size and distance were significant. The microstructure characterizations were carried out by image analysis based on the gray-level distribution of SEM images that present particular and reproducible characteristics related to ceramic phases [17]. Images were processed by ImageJ tools that can perform measurements of objects in images [18]. However, the efficiency of image processing techniques depends on image quality, noise reduction technique, and also on filtration and segmentation techniques to distinguish objects. Particularly, the measurement of particle size requires accurate edge detection between adjacent or overlapping particles, and the use of a segmentation technique was important for the accurate size measurement. The gray level distribution of images was firstly analyzed by simple thresholding, but some phases presenting close level were not accurately separated [19]. Consequently, a watershed segmentation of overlapping and touching particles was used since it efficiently separates irregularly shaped particles [20]. Finally, images resulting from segmentation of grains were summed to images from the thresholding of images, and then a skeleton cleaning process was used to remove remaining noise. Specific attention was devoted to intragranular pores and isolates pixels groups that were considered in grain quantification. Results were validated by visual measurements on images to confirm if they were statistically dependent.

RESULTS

Results of flexural strength are reported in Table III. Values are average data from 90 measurements for each ceramic type (Table II) that ensure the significance of results from brittle materials. G0 was the weakest material, G5 the strongest one, and G10 had an intermediate value. Differences between values were sufficiently large to prove the significance of results that can be correlated to microstructural differences. Table III also reports standard deviations calculated with the whole data sets that evidence the increasing width of data values from G0 to G5 and G10 set of samples.

Table III - Average values of flexural strength and standard deviations for different sample sets.
[Tabela III - Valores médios de resistência à flexão e desvios padrão para os diferentes conjuntos de amostras.]

Sample	Average strength (MPa)	Standard deviation (MPa)
G0	16.8	1.4
G5	23.1	1.9
G10	22.0	2.5

The Weibull statistics (Eqs. A and B) from the large set of samples (90 samples for each) was calculated using the statistical estimator of Eq. C. Besides, the hypothesis of more than one subset of data inside the whole data sets from 90 tested samples was considered, induced by microstructural heterogeneities. Consequently, different simulations with Eq. B were made, using 1 to 3 subsets of data to improve the significance of simulations of experiments. A subset is

Table IV - Weibull parameters of each subset of data P_i in each whole data set, for the 3 studied ceramics. P_i is the relative quantity of data for the subset, m the Weibull modulus and Y_{i0} the Y-intercept.
[Tabela IV - Parâmetros de Weibull de cada subconjunto de dados Pi em cada conjunto de dados, para as 3 cerâmicas estudadas. Pi é a quantidade relativa de dados para o subconjunto, m o módulo de Weibull e Y_{i0} o intercepto em Y.]

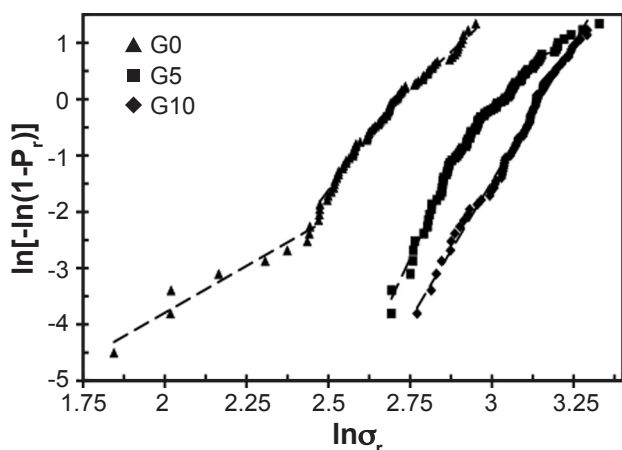| Ceramic type	Subset 1			Subset 2			Subset 3		
	P_1	m_1	Y_{10}	P_2	m_2	Y_{20}	P_3	m_3	Y_{30}
G0	0.133	3.33	10.46	0.600	7.87	21.30	0.267	5.31	14.44
G5	1.000	9.79	30.84	-	-	-	-	-	-
G10	0.422	12.46	37.10	0.500	5.84	17.69	0.078	2.65	7.47

Figure 1: Weibull plot of flexural strength (σ_r) for G0, G5 and G10 ceramics (90 data points) and fit of data, considering the occurrence of 3 subsets of data for G0 and G10 and 1 subset for G5.
[Figura 1: Gráfico de Weibull da resistência à flexão (σ_r) para as cerâmicas G0, G5 e G10 (90 pontos de dados) e ajuste de dados, considerando a ocorrência de 3 subconjuntos de dados para G0 e G10 e 1 subconjunto para G5.]

defined as a family whose members (samples) have similar characteristics. The subset grouping shows these samples have defects of similar nature and shape. All simulations were presented into the Weibull plot (Eq. B), and the best fits of data are presented in Fig. 1. For G0 ceramic, the existence of 3 subsets of data was considered because there were three parts of the plot that were considered linear and represented by a line. For G5, only 1 subset of data was necessary, which the plot was considered linear and represented by a line. For G10, 3 subsets of data were also considered as G0.

Parameters for each subset of data are the relative quantity of data points, the Weibull modulus m and the Y-intercept $-m \ln \sigma_0$. They are reported in Table IV. The sum of the values of P_i tends to 1 (for G0 and G10, $P_1+P_2+P_3=1$ and for G5, $P_1=1$). The simulation got closer to reality. It was seen that Weibull moduli of G0 and G10 were strongly changed when considering different subset of data, whereas for G5 the Weibull modulus had a constant value.

Microstructures of samples are presented in SEM images of Figs. 2a, 2b and 2c for G0, G5 and G10 ceramics, respectively. It was acquired numerous SEM micrographs for image analyses and typical examples of images in backscattering electron (BSE) mode for each ceramic are shown in these figures. The first information obtained from image analyses is the area density of the different phases. The calculated data were the ratio of the pixel number from a given phase on the total pixel number. The accuracy of this ratio depends on the thresholding procedure and it was high for the porosity ratio since the large difference in grey levels. Results of porosity in Table V reveal the role of talc addition in porosity reduction. The grain size was measured for the 3 samples by a sequence of usual morphological operations including segmentation. It led to values in Table V, revealing that grain size distribution was only slightly changed with 5 wt% of talc addition (G5), but the size distribution was enlarged towards the larger size for 10 wt% of talc (G10). Finally, the microstructural information was completed by the quantification of the grain interconnectivity that was more easily obtained from the pore interconnectivity from thresholded images [21]. The procedure necessitated the counting of nodes that were joint points between continuous pore domains, which was applied to mineral resources
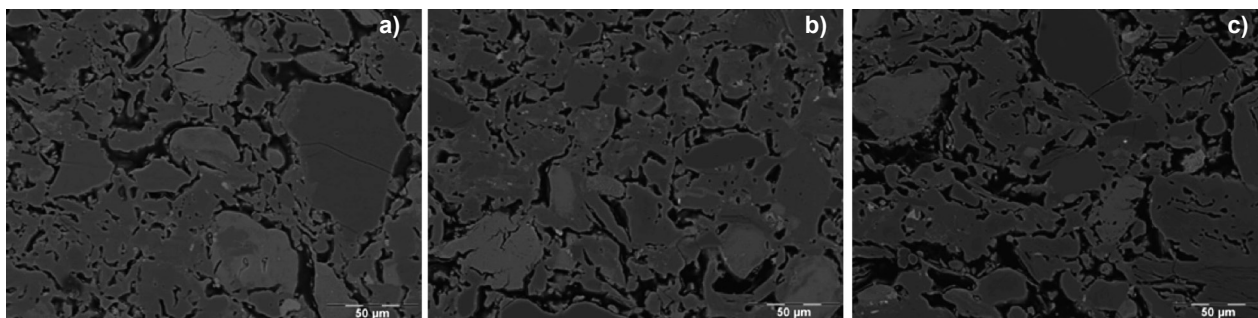

Figure 2: Typical SEM-BSE images showing microstructure of G0 (a), G5 (b), and G10 (c) ceramics.
[Figura 2: Imagens típicas de MEV-BSE mostrando a microestrutura das cerâmicas G0 (a), G5 (b) e G10 (c).]

Table V - Porosity, grain size, ratio of interconnected pore domains and fracture toughness for the 3 ceramic samples.
[*Tabela V - Porosidade, tamanho de grão, razão de domínios de poros interconectados e tenacidade à fratura para as 3 amostras de cerâmica.*]

Ceramic type	Porosity (vol%)	Range of grain size (μm)	Pore interconnectivity (%)	Toughness (MPa.m$^{0.5}$)
G0	66.4±2.6	32-124	89	0.09-0.19
G5	46.6±2.1	28-95	64	0.12-0.22
G10	64.0±3.1	21-153	73	0.10-0.27

[22]. Results are the ratio of the number of pore domains containing at least one node over the total number of pore domains (Table V). In that way, isolated pore domains were within areas where the grain interconnections predominated. The value of fracture toughness, K_{Ic}, was calculated with Eq. E from flexural strength in Table III and from grain size in Table V that were obviously equivalent to elongated pore length along grains in microstructures. Ranges of toughness are reported in Table V.

DISCUSSION

Microstructural characteristics of G0 (Fig. 2a), G5 (Fig. 2b) and G10 (Fig. 2c) samples were very different. It came from talc addition that reacted with clay during firing. New phases as enstatite appeared progressively above 900 °C in accordance with the SiO_2-Al_2O_3-MgO ternary diagram [23]. Beside recrystallization, MgO additions to clay reduce both the formation temperature of the liquid phase above 1000 °C and the viscosity of the glassy phase [24]. It changes both the strength, the firing shrinkage and the water absorption [25]. Talc additions also induced strong microstructural data change (Table V). With our compositions, both porosity, grain size range and pore shape were effectively changed. In general, microstructures of the 3 samples showed large pores that were mostly elongated along bigger grains and had interconnections between them. Positions and shapes of Weibull plots in Fig. 1 evidenced that fracture statistics were related to microstructural characteristics and then to flaw populations in the heterogeneous microstructures of Fig. 2.

For G5, the plot of data in Fig. 1 was aligned along a quasi-straight line and was, therefore, Weibull distributed. It means that the flaw size range had a unimodal distribution with size reported in Table V. Using Weibull statistics, it is possible to calculate the failure probability for different strength values even it is outside the experimental range. Microstructural analyses of G5 also evidenced that both the grain size range and the pore interconnectivity had the lowest values. They reflected a more homogeneous microstructure and correspondingly a relatively high Weibull modulus (m=9.79). For G0 and G10 at the low-stress side, the defect populations were that of Weibull materials. At intermediate stresses, the distribution moved from one line to another. At higher stresses, a lower slope (G0) or a higher slope (G10) meant either a larger scatter of strength data for G0

and a reduced one for G10. They reflected the occurrence of different defect populations in each sample. The stress-dependent Weibull modulus meant that the occurrence of a Weibull behavior remained valid only in limited stress ranges. A similar behavior and Weibull multistep characteristics were reported for zirconia ceramics having different surface treatment after sintering [26]. They were able to create supplementary surface defect populations that occurred besides the initial volume defect population. However, our samples were different since populations of defects were supposed to occur simultaneously during sintering in the sample volumes, and their identification was not so explicit. Table IV reports a high value of modulus (m_1=12.46) for the lower stress range of G10. Similar behavior was seen in the intermediate stress range of G0 (m_2=7.87). Since m values strongly changed with stress, they should be correlated with grain size range and pore interconnectivity (Figs. 2a and 2c). From Table V, G0 and G10 samples appeared more heterogeneous and correspondingly different multistep responses were obtained.

In all ceramics, the Griffith criterion predicts that a crack-like flaw becomes critical if its stress intensity factor exceeds the fracture toughness, K_{Ic}. Assuming a Weibull-like distribution of flaws, average toughness values for the three samples are reported in Table V. They were very low and within relatively large intervals, but similar to those reported for common and brittle ceramics obtained from clay and talc [27]. Despite the scatter of results, Table V also shows that the Weibull model is satisfactorily when elongated pores are assimilated to cracks. However, questions arise from the multistep response of G0 and G10 samples since toughness can be changed against the applied load. For G0 sample, the increase of Weibull modulus at higher stress should be from the increase of toughness that should mean the occurrence of an R-curve behavior. Finally, it is shown that the Weibull modulus varied with the applied load, and the response of materials in all applications must be considered within the load range of subset of data in Table V. According to [5], a value of m=7 for a relatively large specimen means that only surface flaws are significant in fracture. For a relatively small specimen, m value is able to increase up to 15, and volume flaws can be supposed to cause a fracture. Such behavior is often observed during the use of ceramic products meaning that the behavior of all fragile ceramic products cannot be fully described by a Weibull analysis.

CONCLUSIONS

The Weibull distribution model is very commonly used in the study of brittle ceramics but remains a controversial question since it implies some arbitrary assumptions. For the 3 clay-talc samples studied, we showed that shapes of Weibull distribution were not effectively related to material compositions but to microstructural characteristics. Beside grain and pore sizes and distributions, we considered interactions among large pores assimilated to large cracks, as evidenced on SEM images. Interconnections between pores formed a network of possible failures under the stress field, resulting in a change of the shape of Weibull plots. They were the complex results of microstructural defects as pores and pore interconnections. When both the grain size range was reduced and when limited pore interconnectivity occurred, a more homogeneous response under a large range of loading was obtained.

ACKNOWLEDGMENTS

REFERENCES

[1] K. Traoré, T.S. Kabré, P. Blanchart, Appl. Clay Sci. **17** (2000) 279.

[2] X. Zhang, J. Knott, Acta Mater. **48**, 21 (2000) 35.

[3] Ch. Fiał, A. Ciaś, A. Czarski, M. Sułowski, Arch. Metall. Mater. **61**, 3 (2016) 1547.

[4] L. Ćurković, A. Bakić, J. Kodvanj, T. Haramina, Trans. Famena **34**, 1 (2010) 13.

[5] R. Dancer, P. Supancic, J. Pascual, T. Lube, Eng. Fract. Mech. **74** (2007) 2919.

[6] C. Lu, R. Danzer, D. Fishcer, Phys. Rev. E **65** (2002) 67102.

[7] S. Kam, L. Zerbo, S. Mohamed, J. Soro, K. Traoré, J.D. Bathiebo, Y. Millogo, R. Ouédraogo, M. Gomina, P. Blanchart, J. Soc. Ouest-Afr. Chim. **27** (2009) 67.

[8] S. Kam, L. Zerbo, J.D. Bathiébo, J. Soro, S. Naba, U. Wenmenga, K. Traoré, M. Gomina, P. Blanchart, Appl. Clay Sci. **46**, 4 (2009) 351.

[9] W. Weibull, J. Appl. Mech. **18**, 3 (1951) 293.

[10] K. Charlet, J.P. Jernot, M. Gomina, L. Bizet, J. Bréard, J. Compos. Mater. **44** (2010) 2887.

[11] R. Danzer, T. Lube, P. Supancic, Z. Metallkd. **92** (2001) 773.

[12] M. Elgueta, G. Diaz, S. Zamorano, P. Kittl, Mater. Design **28** (2007) 2496.

[13] U. Jansen, D. Stoyan, Granul. Matter **2** (2000) 165.

[14] M. Bebbington, C.-D. Lai, R. Zitikis, Reliab. Eng. Syst. Safe. **92** (2007) 719.

[15] K. Boussois, N. Tessier-Doyen, P. Blanchart, J. Eur. Ceram. Soc. **34**, 1 (2014) 119.

[16] G.D. Quinn, J. Salem, I. Bar-on, K. Cho, M. Fotey, H. Fang, J. Res. Natl. Inst. Stand. Technol. **97**, 5 (1992) 579.

[17] A.N. Diógenes, E.A. Hoff, C.P. Fernandes, in 18th Int. Congr. Mech. Eng., Ouro Preto, Brazil (2005).

[18] C.A. Schneider, W.S. Rasband, K.W. Eliceiri, Nat. Methods **9**, 7 (2012) 671.

[19] P. Belhomme, D. Houivet, W. Lecluse, J.M. Haussonne, J. Eur. Ceram. Soc. **21** (2001) 2149.

[20] Rishi, N. Rana, Int. J. Eng. Res. Technol. **4**, 11 (2015) 247.

[21] H. Harrar, L. Hamami, J. Med. Bio. Eng. **33** (2012) 569.

[22] Y. Chen, M. Mastalerz, A. Schimmelmann, J. Microsc. **256**, 3 (2014) 177.

[23] W. Schreyer, J.F. Schairer, J. Petrol. **2** (1961) 324.

[24] M. Valášková, Ceramics-Silikáty **59**, 4 (2015) 331.

[25] Z.B. Ozturk, N. Ay, J. Ceram. Process. Res. **13**, 5 (2012) 635.

[26] F.T. da Silva, M.A.N. Zacché, H.S. de Amorim, Mater. Res. **10**, 1 (2007) 63.

[27] P. Sin, R. Veinthal, F. Sergejev, M. Antonov, I. Stubna, Mater. Sci.-Medzg. **18**, 1 (2012) 90.